Microseismic Motivated Model for Asymmetric Hydraulic Fractures in Adjacent Multiple Transverse Fracture Horizontal Wells

A Thesis

Presented to

The Faculty of the Department of Petroleum Engineering

University of Houston

In Partial Fulfillment

Of the Requirements for the Degree

Master of Science

In Petroleum Engineering

By

Xiaofan Hu

December 2018

Microseismic Motivated Model for Asymmetric Hydraulic Fractures in Adjacent Multiple Transverse Fracture Horizontal Wells

Xiaofan Hu

Approved:

Chair of Committee
Dr. Christine Ehlig-Economides,
Professor, Petroleum Engineering

Committee Members:

Dr. Egor Dontsov
Assistant Professor, Civil and Environmental Engineering

Dr. Guan Qin
Associate Professor, Petroleum Engineering

Dr. Suresh K. Khator, Associate Dean,
Cullen College of Engineering

Dr. Mohamed Y. Soliman,
Professor and Director,
Petroleum Engineering Department

Dedication

To those who sacrificed during 2015-2018 oil down turn,

may you be as strong and resilient as our industry.

Acknowledgment

First, I would like to express my gratitude to my committee chair, Dr. Christine Ehlig-Economides for her patience and support throughout my research, and more importantly, for leading and guiding me during the Oil and Gas industry downturn.

I would also like to thank my committee members, Dr. Egor Dontsov and Dr. Guan Qin for their valuable and insightful advices on my research.

I would also like to extend tremendous thanks to Dr. Guoqing Liu, without whom this research would not have been possible.

I want to thank my wife Chenchen Feng, the rock of our family, for taking care of me and my lovely daughter Ivy. I am also thankful for my daughter for bringing happiness to our family. I also want to thank my parents and in-laws for their support.

My appreciation must also go to Dr. Yunhui Tan for the discussions about microseismic and hydraulic fracturing and I regretted not to talk to him earlier. Special thanks go to Dr. Chen Qi for helping me with programing and for his friendship. My deep thanks go to Dr. Qiuliang Yao for discussions on hydraulic fracturing, and for his help with my progress in America. Thanks also go to Guofan Luo, Yan Song, Yao Tian, Masha Bybh and Nadia Menouar for their help and support.

I want to thank all my friends and former colleagues in different corners of the world; I would not be here without your sacrifice. I wish you and your families well.

At last, my thanks must also go to Houston traffic for providing me abundant time for thinking and crafting my thesis while driving!

Microseismic Motivated Model for Asymmetric Hydraulic Fractures in Adjacent Multiple Transverse Fracture Horizontal Wells

An Abstract

Of a

Thesis

Presented to

The Faculty of the Department of Petroleum Engineering

University of Houston

In Partial Fulfillment

Of the Requirements for the Degree

Master of Science

In Petroleum Engineering

By

Xiaofan Hu

December 2018

Abstract

Engineers commonly expect symmetric fracture wings in multiple transverse fracture horizontal wells (MTFHWs). However, microseismic surveys have shown asymmetric hydraulic fracture growth of in successive MTFHWs, and the reason may be elevated stress around a recently fractured well. Dissipating net pressure from the first fracturing treatment may increase the minimum principal stress near created fractures and cause fractures being pumped from an adjacent horizontal well to grow away from the previous fractures and toward lower minimum principal stress on the opposite side of the well.

Microseismic maps have shown uneven fracture propagation in a treatment well very near a recently fractured well. Motivated by the microseismic observations, we developed a simple 2-D fracture model to simulate asymmetric fractures which can approximately simulate fracture propagation with a lateral stress barrier.

The model indicates a preferred order for hydraulic fracturing in multiple wells that minimizes or avoids asymmetric fracture wings.

Table of Contents

List of Figures

List of Tables

Nomenclature

A_f: fracture face area, ft^2

$A_{ft,prop}$: proppant fracture face area, ft^2

c_L: leak-off coefficient, $ft/min^{0.5}$

c_f: fracture compliance, ft/psi

d: distance to the elevated zone, ft

g_0: loss volume function at $\Delta t_D = 0$, dimensionless

h_f: fracture height, ft

p_{net}: net pressure, psi

q_i: pump rate at i^{th} time, bbl/min

r_p: Ratio of permeable fracture surface area to the gross fracture area, dimensionless

t: treatment elapse time, min

t_i: i^{th} time

$t_{i,prop}$: i^{th} proppant time

V_f: total fracture volume, ft^3

$V_{leakoff}$: leakoff volume, ft^3

V_{total}: total pumping volume, ft^3

x_f: fracture half-length, ft

α: area exponent before and after shut-in, dimensionless

σ_x: stress in x direction, psi

CHAPTER 1

Introduction

Microseismic events offer the leading mechanism to visualize the geometry and propagation of hydraulic fractures during a fracturing treatment. The discrepancy between the modeled hydraulic fractures and the ones observed from microseismic monitoring draws attention and deserves more investigation. In this chapter, we will start with background information for this study. Then we will present the thesis research objective and summarize this chapter.

1.1. Background

In this section, we will highlight microseismic observations of asymmetric fractures, consider the impact of fracture asymmetry on well production, and review existing hydraulic fracturing models.

1.1.1. Microseismic Observations

The microseismic survey is a widely used hydraulic fracturing treatment visualization tool. It can provide 3-D location, time, magnitude, and source mechanism of fracture slippage (shear motion), aperture change (tensile motion), and combinations of the two (Duncan 2010). Detected motions are mainly caused by activation of existing healed fractures in the rock that tend to occur beyond the tip of or aside propagating hydraulic fracture planes (Warpinski et al., 2013). The cluster of microseismic events near a propagating hydraulic fracture provides an indirect indication of its areal and vertical extent. An envelope around the microseismic events for multiple hydraulic fracture stages of a MTFHW provide an estimate of the maximum stimulated rock volume (SRV) that the well can drain (Gaurav and Kashikar 2015). Interference between closely spaced wells may limit the actual well drainage volume to less than the SRV indicated by a microseismic survey. Microseismic based fracture attributes can help operators improve hydraulic fracturing treatment designs.

Figure 1 shows microseismic data from the Duvernay Formation presented by Stephenson (Stephenson et al., 2018). There are two wells in this project (Figure 1a), the first drilled in the minimum stress (NW-SE) direction and hydraulically fractured using gelled fracturing fluid, and the second drilled in a NS direction and fractured using slick water shortly after the first well was fractured. The first well has 16 perf-and-plug stages, and the second well has 17 perf-and-plug stages. Figure 1b shows envelopes around microseismic data clouds for each stage. The gray color represents microseismic events belonging to the first well and the light blue presents microseismic events from the second well. The red and black colors indicate microseismic event overlaps between adjacent stages.

Figure 1 enables several observations. First, the microseismic event clouds cluster around parallel lines, suggesting that there is no change in the minimum stress direction, neither from stress shadowing effects on successive stages, nor from stress alteration from one well to the next. The event clouds do not bend or curve due to previously fractured stages and do not realign due to a previously fractured well. The overlapped stages suggest that successive hydraulic fracture stages initiate or reinitiate shear events in already altered rock volumes.

Second, and more importantly for this study, the microseismic event geometry for the second well was influenced by the first well in a manner not predicted by published models. The hydraulic fractures from the first well were symmetric on each side of the wellbore from toe stages to heel stages. In contrast, events for the second well suggest longer asymmetric hydraulic fractures. Fractures near the toe of the second well have shorter half-length in the SW direction, but fractures near the heel of the well have shorter half-length in the NE direction. Not shown in the figure, but shown in the conference presentation, are previously fractured wells drilled in the minimum stress direction to the SW of the second well that may explain the asymmetric fracture growth near the toe of the well. The apparently asymmetric behavior of fractures at the heel and toe of the well are evidence that motivate the model developed for this study. Fractures created along the middle of the drilled horizontal length show nearly symmetric growth perhaps unimpaired by any of the surrounding wells or reflecting symmetric stress alteration.

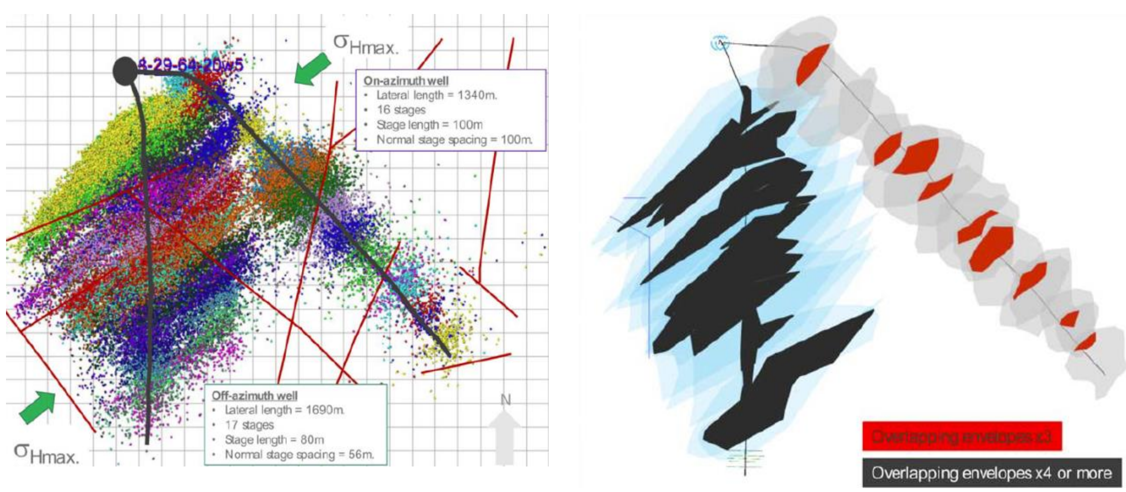

(a) (b)

Figure 1: Microseismic results from Duvernay Shale. (a) Microseismic data are colored by stage; (b) Envelop of microseismic results, darker color represents the area overlapped by microseismic events from different stages (Stephenson et al., 2018).

The above example shows apparent fracture growth away from a recently fractured well. Walser and Siddiqui (Walser and Siddiqui 2016) also observed asymmetric fractures due to an opposite scenario. In Figure 2 the asymmetric fracture growth is toward a well that has been on production before the second well showing microseismic events was hydraulically fractured. The authors suggested that some unconventional horizontal plays experience asymmetric fractures trending towards the rock volume with lower pressure caused by a depleted well, typically a parent well or pilot well, near the treatment well. We note that the figure shows that microseismic events are much more frequent in the direction away from the wells containing the borehole geophone arrays; hence, it is unlikely that the event pattern was an artifact of sensor locations.

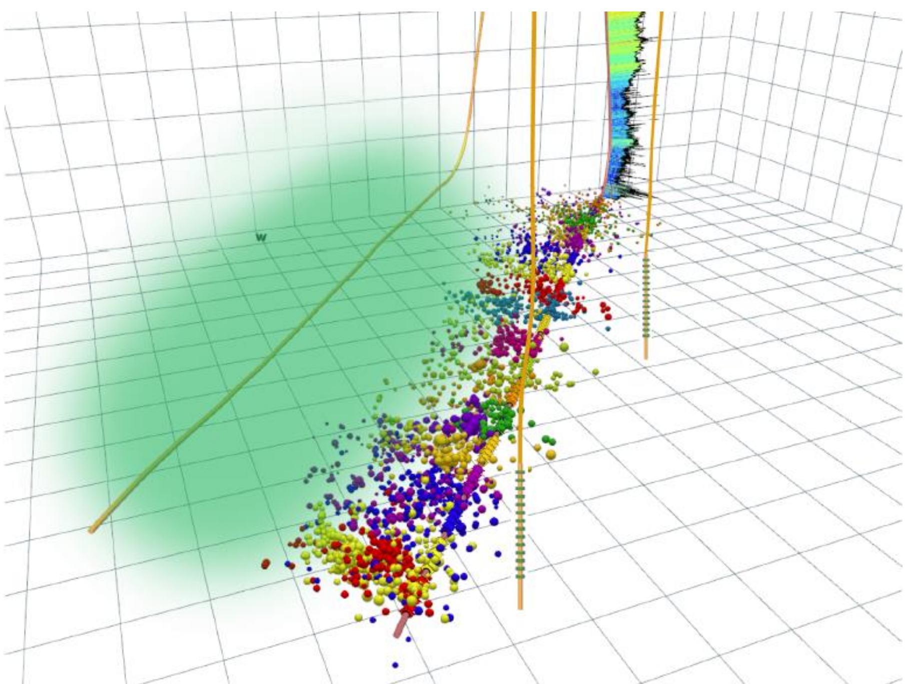

Figure 2: Shows microseismic results indicating asymmetric fractures towards a lower pressure formation (Walser and Siddiqui 2016).

Microseismic event maps may extend much further than the extent of propped hydraulic fractures. Because microseismic events relate to shear, and proppant is placed mostly in tensile fractures, the microseismic technique does not see proppant directly. However, the timing of events may indicate which events more closely relate to proppant placement. Figure 3 from Tan (Tan 2015) illustrates microseismic events recorded during a fracture treatment. The circle radius corresponds to the magnitude of the seismic event.

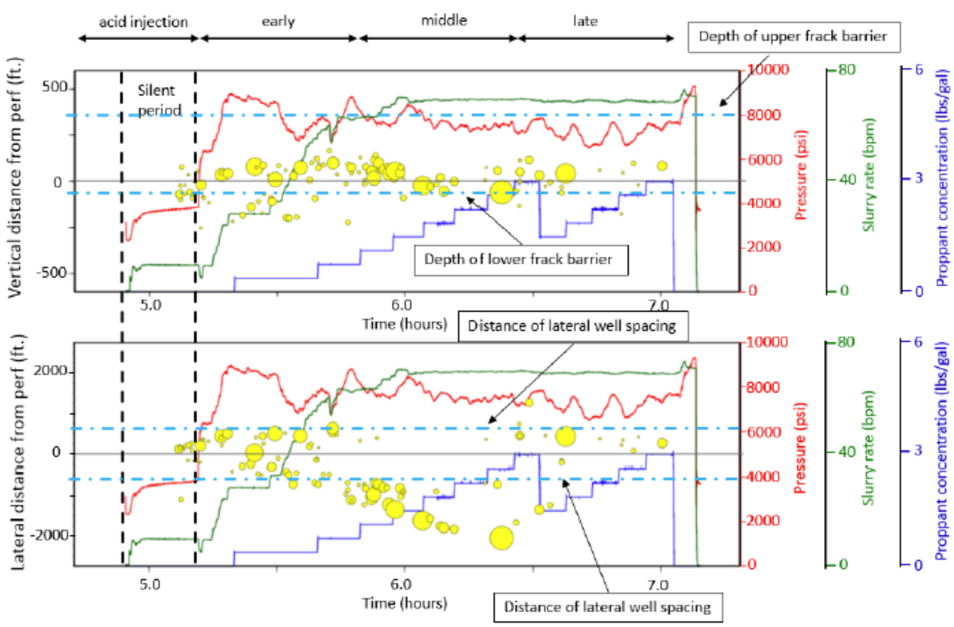

Figure 3: Shows the distance from the microseismic events to the stage center. The top plot shows the vertical distances and the bottom plot shows the horizontal distance. The background red, green and blue curves are the treating pressure, slurry rate and proppant (Tan 2015).

McKenna (McKenna 2014) used microseismic events to guide generation of a discrete fracture network (DNF) and then labeled propped and unpropped networks shown in Figure 3 with propped fracture events occurring during proppant slurry injection. In general, the extent of the propped DFN is much shorter and constrained than the extent of the unpropped DFN. The modeled proppant distribution in hydraulic fracture was verified by Treatment Design Analysis shown in Figure 4. This figure distinguished between events occurring during pad injection (pale bars labeled Slickwater Population) and events occurring during proppant injection (dark bars labeled Proppant Population). In particular, the graphic shows the much shorter distance from the well of the Proppant Population. Figure 5 suggests that the microseismic cloud may extend much further than the extent of propped fractures.

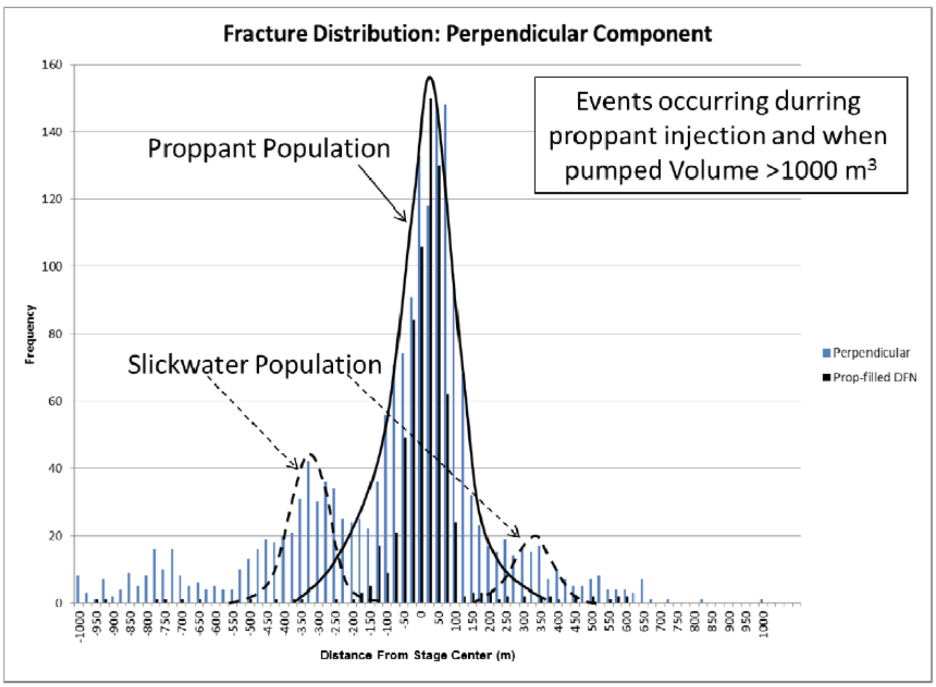

Figure 4: Comparison of proppant population using the perpendicular microseismic location using the treatment design analysis approach where microseismic events are limited to events occurring during proppant injection and when pumped slurry volume is > 1000 m3 (blue histogram) to modeled proppant-filled Discrete Fracture Network modeling approach (black histogram). Proppant population can be separated from slickwater population by assuming that two populations exist and are normally distributed (McKenna 2014).

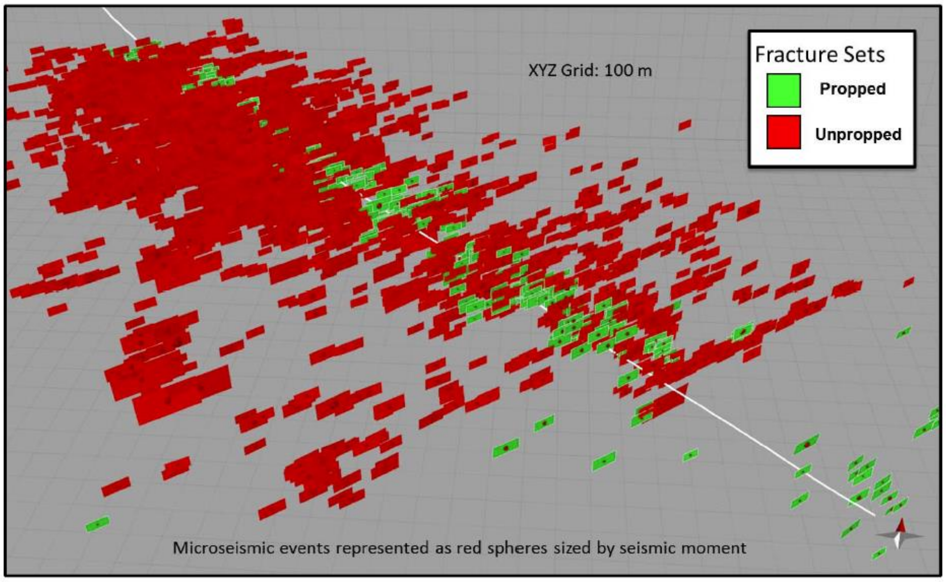

Figure 5: Microseismic derived Discrete Fracture Network, each sphere is represented by a microseismic event. The green ones are filled with proppant and the red ones are unpropped (McKenna 2014).

Sometimes, due to lack of understanding microseismic data, or its limitations, the behavior of hydraulic fractures can be misleading. Microseismic can be a useful tool only if we can understand it correctly. We will discuss more about detailed microseismic technology in Chapter 2.

1.1.2. Impact of Asymmetric Fractures on Well Performance

In the previous section, we discussed evidence of asymmetric fractures observed from microseismic data. This section considers the effect of asymmetric fractures on well performance.

Walser and Siddiqui 2016 presented a case study showing that wells having asymmetric fractures will have lower production after 20 years. They simulated one symmetric base case with two identical wells drilled, completed and produced at the same time, a second symmetric base case like the base case except the second well starts production 6 months after the first well, and a third asymmetric case like the second base case except with the entire fracture set of the second well shifted 200 ft towards the well that had been producing for 6 months. The modeled results are shown in Figure 6. Compared to symmetric cases, the asymmetric case has almost the same initial production, and similar cumulative production for the first 5 years. After that, the total production decreased significantly for the asymmetric case. Walser and Siddiqui 2016 indicated that the asymmetrically fractured well would lose approximately 5.6% of total production, or about 886,000 MBO.

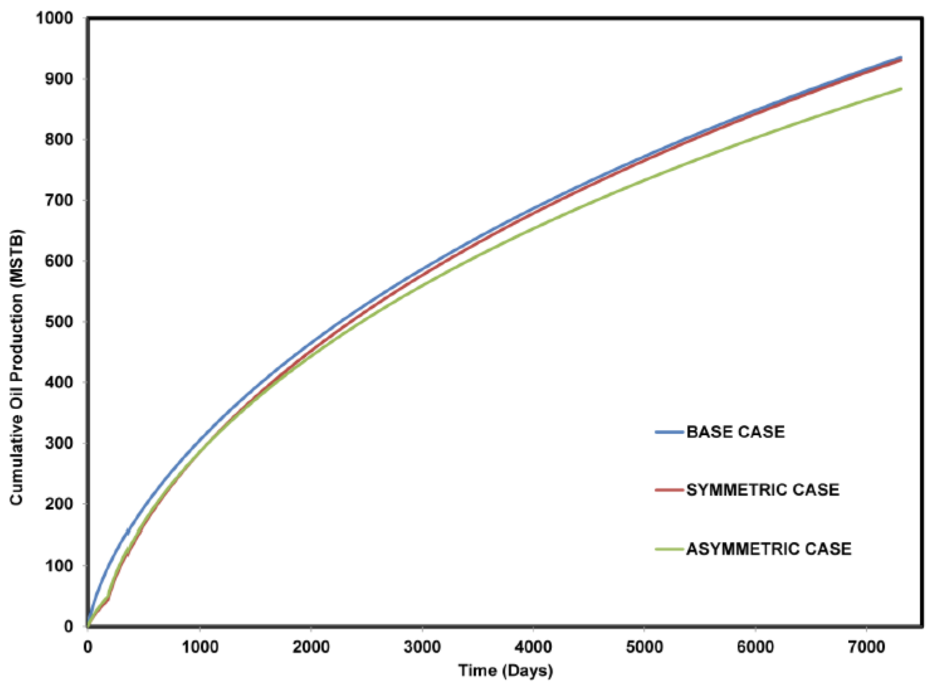

Figure 6: Modeled results showing less production for asymmetric fracture case (Walser and Siddiqui 2016).

1.1.3. Hydraulic Fracture Models

Rahman and Rahman 2010 reviewed hydraulic fracturing models used to predict fracture propagation in the oil and gas industry. The estimated fracture height and length from the fracturing models facilitate well planning and hydraulic treatment design. In general, there are three different types of hydraulic fracture models, 2-D models, Pseudo 3-D models and 3-D models. Each type of hydraulic fracture model has its own advantages and disadvantages. In this section, we will briefly review different hydraulic fracture models.

The 2-D hydraulic fracture models usually fix one dimension of the hydraulic fracture, usually the fracture height, and predict fracture width and the remaining dimension, usually the fracture length) based on material balance under idealized fracture geometries (Rahman and Rahman 2010). Perkins and Kern model (PKN) and Geertsma and de Klerk (KGD) model are the two most popular 2-D fracture models, and their fracture geometries are shown in Figure 7. In the plots, $L(t)$ represents fracture length, $w(x,t)$ is fracture width (where $x = 0$ means fracture width at wellbore), and h_f is fracture height. Further development of 2-D fracture models has accounted for leak-off of pumping fluid into the formation during fracture propagation.

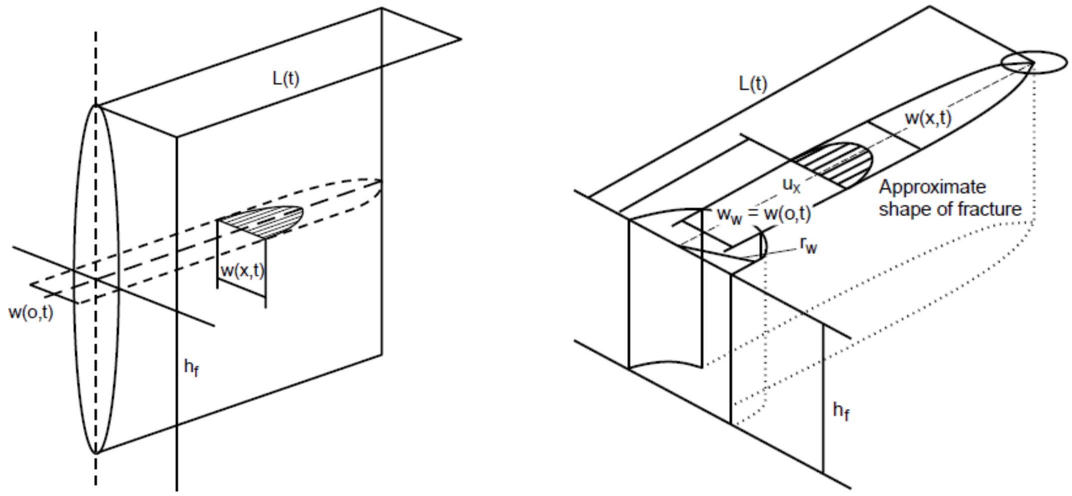

(a) (b)

Figure 7: Classic 2-D hydraulic fracture geometries. (a) is PKN model; (b) is KGD model (Economides and Nolte 2000).

2-D hydraulic fracture models require pumping fluid material balance and constant properties including fracture height and conductivity, fluid viscosity, leak off coefficient, pumping rate, Young's modulus, and Poisson's ratio. 2D fracture models also require a fixed stress field that is laterally homogeneous. Only symmetric hydraulic fractures can be simulated with these models.

Pseudo 3-D fracture models were introduced to simulate asymmetric vertical hydraulic fracture growth in multi-layer formations. Pseudo 3-D fracture models do not simulate fully 3-D fracture growth allowing hydraulic fracture geometry to change freely in 3-D space; instead, they add height variation into 2-D fracture models that keep the same geometry laterally. Newberry (Newberry et al., 1985) introduced one of the methods to let hydraulic fractures grow unevenly in a vertical direction. They used full waveform data from a sonic wireline tool to find the relationship between hydraulic fracture height and the relative stress distribution near it.

Some of the Pseudo 3-D fracture models have shown unrealistic results. Gupta (Gupta et al., 2012) presented a fracture model indicating dramatic changes in fracture azimuth caused by stress reorientation, as shown Figure 8. However, microseismic survey data have not shown evidence of changing fracture orientation.

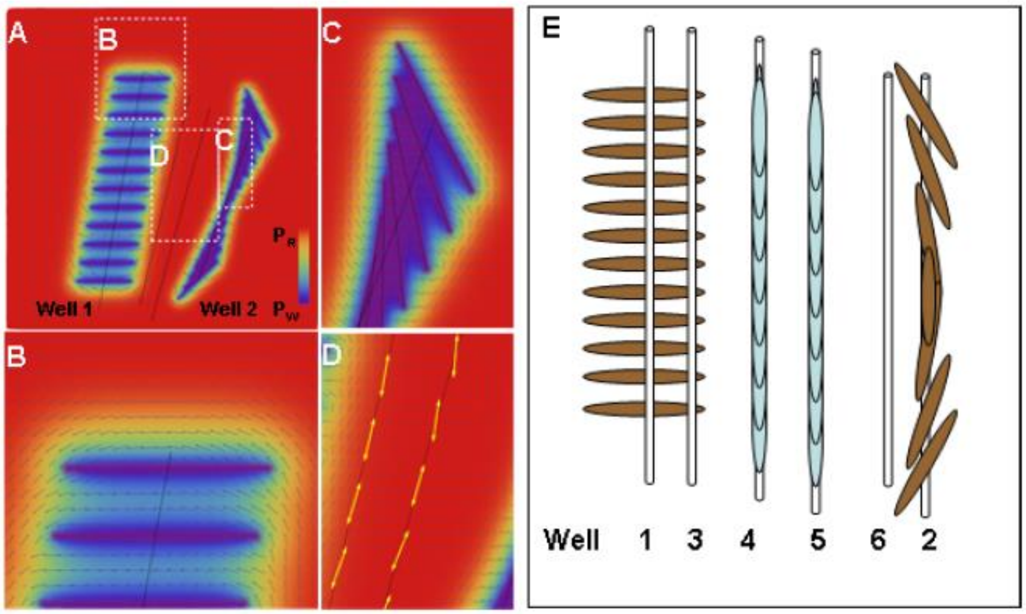

Figure 8: Stress orientation changed dramatically due to presence of fractures from the first well one the left (Gupta et al., 2012).

3-D fracture models are more rigorous for simulating hydraulic fracturing in anisotropic and heterogeneous formations and with more realistic boundary conditions. These models allow simulated fractures to grow freely and allow more complex fracture geometries.

1.2. Research Objective

The objective of this research is to develop a 2-D fracturing model for asymmetric hydraulic fracturing growth in response to lateral stress variation near the horizontal well being fractured.

1.3. Summary

This chapter has provided the motivation for the research objective. Chapter 2 will provide additional detail about microseismic monitoring that helps to explain why asymmetric fracture growth has not been more evident. Then Chapter 3 shows a derivation for a model for asymmetric fracture propagation due to lateral stress imbalance. Chapter 4 suggests approaches to avoid or minimize adverse effects of asymmetric hydraulic fractures. The final chapter offers conclusions and ideas for further work.

CHAPTER 2

Microseismic Hydraulic Fracture Mapping

The background section of Chapter 1 summarized microseismic evidence of asymmetric fracture growth. This chapter provides further detail about microseismic hydraulic fracture mapping.

Microseismic monitoring is a technique to image hydraulic fracture geometry, and contain rock failure information during the treatment (Warpinski et al., 2001). The hydraulic fractures mapped by microseismic surveys during a hydraulic fracturing treatment are important to verify whether created hydraulic fractures achieve the envisioned treatment design. The microseismic event locations and times provide an indication of the hydraulic fracture geometry, and thereby show interactions between fracturing stages and among treatment wells.

There are two types of microseismic surveys, surface or near-surface microseismic monitoring and downhole microseismic monitoring with the difference related to the location of geophones used for receiving seismic signals. Typically, surface microseismic surveys are used for monitoring multiple wells and all of the treatment stages from monitored wells. The surface microseismic monitoring usually requires more than 2,000 geophones in order to provide reliable results. Downhole microseismic surveys often use limited number of geophones monitoring a few stages up to 3,500 ft away from monitor well.

The next three sections will discuss the microseismic technologies and their advantages and disadvantages.

2.1. Surface or Near-surface Microseismic Monitoring

Surface microseismic survey geophones are installed on the ground; Figure 9a shows an array of geophones arranged in a star-shaped pattern. Due to large receiver-source distance and the presence of noise, a typical surface microseismic survey positions thousands of geophones to provide sufficient stack to detect weak signals (Duncan and Eisner 2010). Usually, the treatment wells are below the center of the surface geophone array with sufficiently large array radius to achieve required resolution (Duncan and Eisner 2010). To reduce the surface noise, and therefore, the number of geophones required for monitoring, a near-surface microseismic survey buries the geophones in shallow ground. Surface and near-surface microseismic can be considered as the same method.

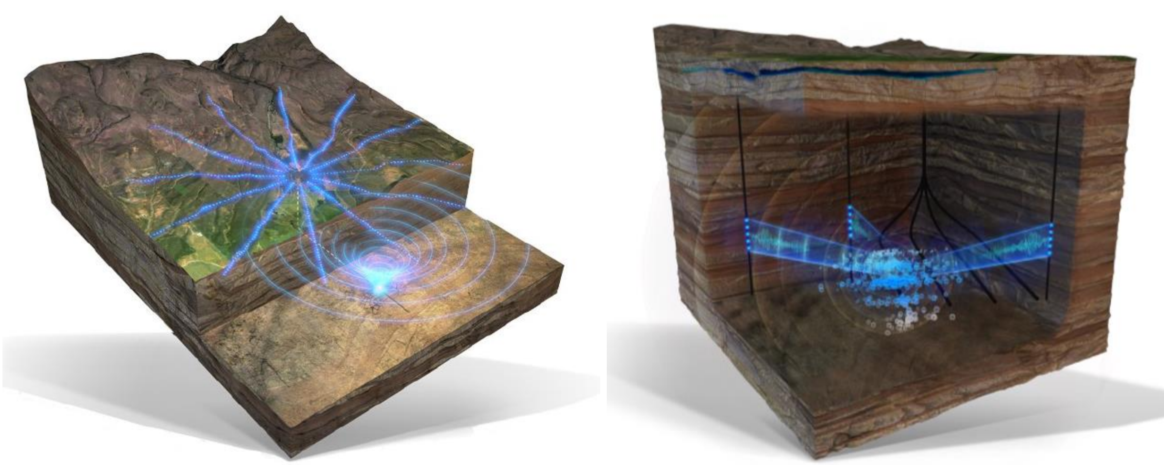

(a) (b)

Figure 9: Microseismic survey acquisition design. (a) is an example of surface microseismic survey which the geophones are placed in the ground. A typical surface microseismic survey has thousands of geophones above the treatment well; (b) is an example of downhole microseismic survey in which the array of geophones is aligned in a nearby well. A typical downhole microseismic survey has about 10-20 geophones. (Source: www.microseismic.com).

2.2. Downhole Microseismic Monitoring

For downhole microseismic the geophones are located in nearby wells. Theoretically, multiple downhole geophone arrays in different wells as shown in Figure 9b yield best results. However, in practice, frequently downhole microseismic surveys use only one monitor well thereby reducing both acquisition and geophysical processing costs. A downhole array commonly has 10-20 3-Component geophones connected by a wire.

Logically more microseismic events would be detected from locations that are closer to the geophones, closer microseismic events with lower magnitude would be detected (Figure 10), giving an impression of a greater number of events per stage in the stages near the monitor well than in the ones farther away. The hydraulic fracture geometries from near-stages and far-stages might be misinterpreted because of contrasts in downhole microseismic event detectability.

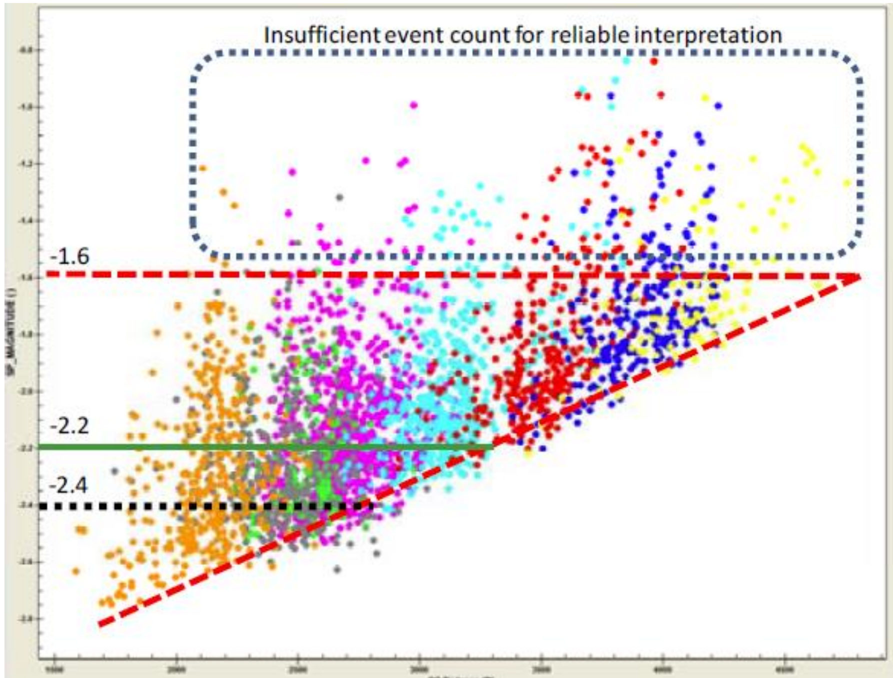

Figure 10: Shows the relationship between monitoring distance verse detected microseismic magnitude. The x-axis is the monitoring distance which is the receiver-source distance; the y-axis the microseismic magnitude which represent the size of each microseismic each microseismic event. The microseismic events are colored by stage. The stages closer to the monitor well have larger number of microseismic events and much smaller microseismic can be detected and located (Cipolla et al., 2011).

Figure 11 illustrates uncertainty in microseismic event locations based on only one monitoring well. The green shaded arcs outline the uncertainty in event locations. Figure 12 illustrates a radius inside which event locations are reliable and outside which the events should be considered invalid.

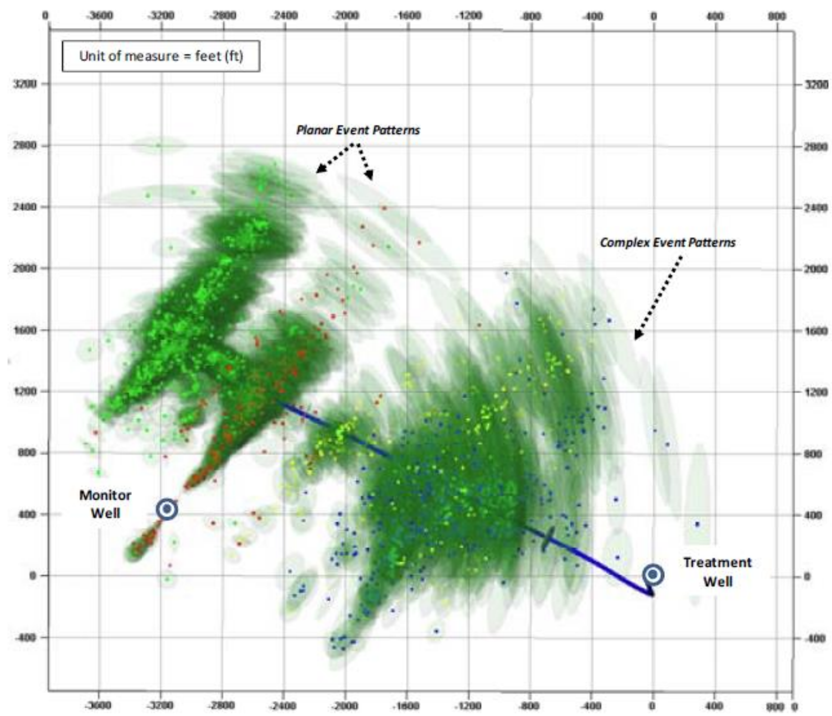

Figure 11: Shows azimuthal uncertainty of microseismic events due to monitor-and-treatment well geometry (Cipolla et al., 2011).

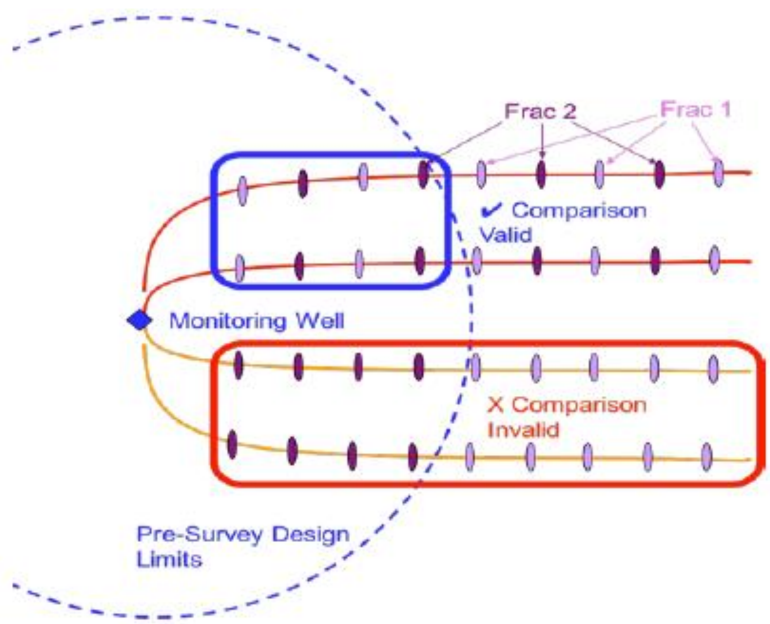

Figure 12: Shows the valid microseismic events for comparison (Maxwell 2012).

For downhole microseismic monitoring, the imaged event locations must be corrected for monitoring well bias including both distance and azimuth. Otherwise, the interpreted failure mechanisms, fracture treatment stimulated volumes and other derived data could be misinterpreted (Cipolla et al., 2011). Figure 13 illustrates how monitoring distance and azimuth bias affects the number of microseismic events detected from each stage or well, microseismic event uncertainty, and microseismic event location alias.

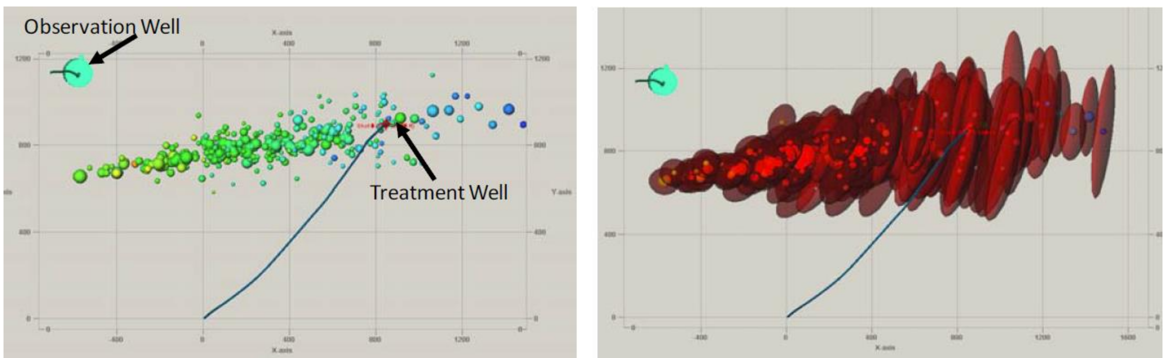

Figure 13: a) shows microseismic event results. The hydraulic fracture represented by microseismic is narrower in the west and wider in the east; b) shows the same microseismic events by ellipsoid. The radius of ellipsoid is proportional to corresponding microseismic event location uncertainty. Both plots are map view (Cipolla et al., 2011).

Fewer microseismic events may be detected from more distant stages, and the detected events are also expected to have higher uncertainties. Considering imaged microseismic events without correction for bias, the mapped hydraulic fracture in 3a appeared narrow in the west and wider in the east. Figure 13b is the same microseismic events but plotted with uncertainty values, the larger the ellipsoid, the bigger uncertainties. These uncertainties mean the actual geometry of this hydraulic fracture may be different from what is apparent in Figure 13a.

2.3. Advantages and Disadvantages to Monitoring Technologies

Both surface microseismic and downhole microseismic surveys have advantages and disadvantages. Operators usually choose one or the other depending on project goals, number of treatment wells, available monitor wells and budget.

Because of receiver-source geometries, surface microseismic typically detect fewer events compared to downhole microseismic monitoring with geophones located closer to the source events. However, surface monitoring can provide the rock failure mechanism for each microseismic event. Further, for surface monitoring, the microseismic event errors and uncertainties are consistent, that is, not dependent on distance between event locations and a downhole sensor array. Unbiased microseismic event locations are crucial for analyzing hydraulic fracture the geometries and fracturing interactions between stages and wells.

The large number of geophones to be laid out for surface acquisition increase both operational cost and permitting dramatically if only one or two wells are to be monitored. However, per unit cost for surface microseismic becomes much cheaper than for downhole microseismic monitoring when multiple wells or pads are to be monitored.

A key advantage of downhole microseismic acquisition it much lower cost, but frequently the results are not consistent. The apparent geometry of imaged hydraulic fractures, or microseismic locations, could be affected by the monitor-and-treatment-well geometry. As shown in Figure 11 and Figure 12, azimuthal uncertainty causes the imaged microseismic event to circle around the monitor well. Without accounting for the azimuthal uncertainties, the hydraulic fracture could appear to be bending, and this could lead to misdiagnosis of an apparent stress shadowing effect. Therefore, to better utilize the microseismic information, we need to know the monitor-and-treatment-well geometry, and whether the data were corrected for location and azimuthal uncertainties.

Except for Figure 2, the microseismic surveys shown in Chapter 1 were all acquired with surface or near-surface microseismic event monitoring. Therefore, the apparent geometries are not subject to bias that may occur for downhole seismic surveys and likely correctly show evidence of asymmetric fracture growth. Further, characterization of the rock failure mechanisms suggests that contrasts in stress may cause the observed asymmetric fracture growth.

2.4. Lack of Published Evidence for Asymmetric Hydraulic Fractures

In the published domain, not many papers focus on analyzing microseismic monitoring of hydraulic fracture interactions between wells, and three main reasons may explain why. Firstly, relatively few microseismic surveys have been published because the high cost of these data makes operators want to keep them confidential. Secondly, because the published data usually lack details indicating to which well microseismic events belong, impact of a nearby well on the acquired data may not be evident. Thirdly, microseismic surveys can be acquired with downhole sensors or surface or near-surface sensors. Because the monitoring distance for data acquired from downhole surveys is typically limited to 3500 to 4000 ft, these surveys are typically limited to one well. Usually only surface or near-surface microseismic surveys have the capability to monitor multiple wells.

This author has seen unpublished evidence of asymmetric hydraulic fractures in successive development wells that originally motivated the interest in doing this work.

2.5. Summary

In this chapter, we summarized different microseismic technologies and their important features. As we described, surface microseismic monitoring provides more consistent results for comparing hydraulic fractures from multiple wells. Analysis of events monitored with downhole microseismic acquisition must carefully consider potential for measurement bias that could lead to artifacts in apparent hydraulic fracture event geometries.

The next chapter shows development of a new fracture model that can simulate asymmetric fracture propagation.

CHAPTER 3

Asymmetric Fracture Model

Chapter 1 showed microseismic evidence of asymmetric hydraulic fractures occurring when stress magnitudes are different in opposing directions from the well and reviewed existing hydraulic fracture propagation models. We adopt a traditional 2-D fracture model in this chapter to develop a new model to simulate asymmetric hydraulic fracture propagation.

3.1. Model Development

In Chapter 1, we observed microseismic survey evidence of asymmetric fracture growth in a well drilled and fractured near the recently fractured well. We hypothesize that hydraulic fracturing elevates minimum stress within a zone enveloping the well. Further we hypothesize that propagation of hydraulic fractures generated subsequently from a nearby horizontal well will be arrested by the elevated stress, and remaining injected fluid and proppant will flow into the fracture wing propagating in the opposite direction.

This section will start by showing the stress elevation occurring in a zone surrounding hydraulic fractures generated from a horizontal well. Then we will present an adapted 2-D model of fracture propagation in a second well with a parallel horizontal trajectory.

3.1.1. Stress Elevation

In this section, we will justify elevated stress around parallel hydraulic fractures that will not relax until well flowback occurs.

Sneddon 1946 modeled the impact on the formation stress caused by an elliptically shaped crack. From Sneddon, the elevated stress, σ_x, can be expressed as

$$\frac{1}{2}\left(\sigma_y - \sigma_x\right) = \Delta p_{net} \frac{r}{c}\left(\frac{c^2}{r_1 r_2}\right)^{3/2} \cos\theta \ \cos\left[\frac{3}{2}(\theta_1 + \theta_2)\right], \tag{1}$$

$$\frac{1}{2}\left(\sigma_y + \sigma_x\right) = \Delta p_{net} \left[\frac{r}{\sqrt{r_1 r_2}} \cos\left(\theta - \frac{1}{2}\theta_1 - \frac{1}{2}\theta_2\right) - 1\right], \text{ and} \tag{2}$$

$$\tau_{xy} = -\Delta p_{net} \frac{r}{c}\left(\frac{c^2}{r_1 r_2}\right)^{3/2} \cos\theta \ \sin\left[\frac{3}{2}(\theta_1 + \theta_2)\right], \tag{3}$$

where Δp_{net} is the net pressure inside the existing hydraulic fracture; r_1, r_2, r, θ_1, θ_2, θ and c are described in Figure 14. For this approach, we need to make the following assumptions (Liu 2015):

1) The crack has an elliptical shape;
2) The crack is very thin ($-c \le y \le c, x = 0$) in the interior of an infinite elastic solid, as shown in Figure 14;
3) The boundary conditions at $x = 0$ are as follows.
    a. There is no shear stress along y axis.
    b. A Griffith crack is opened under the uniform internal pressure. Griffith crack is a very thin crack in the interior of an infinite elastic solid (Sneddon and Elliott 1946).
    c. The strain along y axis beyond crack tips is 0.

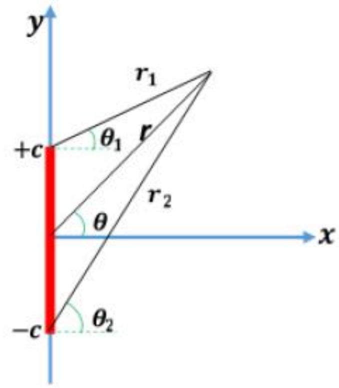

Figure 14: Coordinate of fracture in Sneddon 1946 Model. The red line represents a hydraulic fracture along with the y direction. (Liu 2015)

The result of Equation (3) is shown in Figure 15. The opening of a fracture will cause very high horizontal stress near the fracture that extends horizontally in the direction normal to the fracture plane and decreases dramatically away from the fracture tips in the direction aligned to the fracture plane.

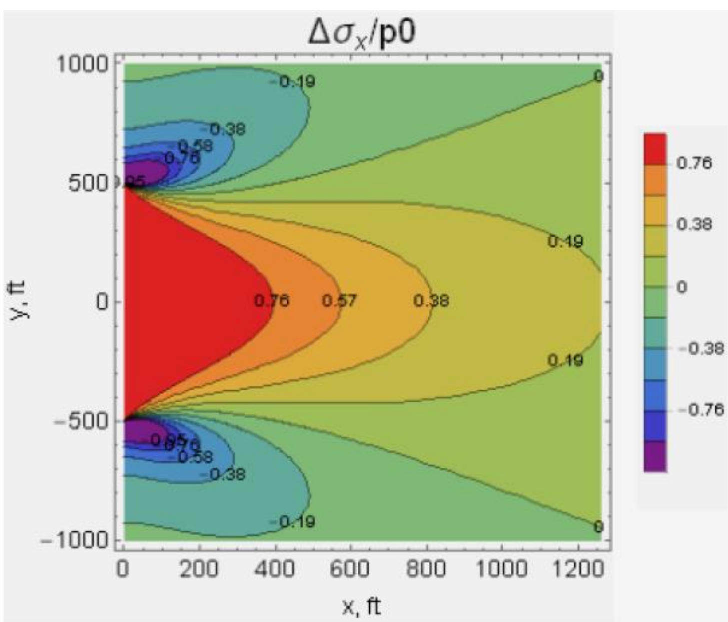

Figure 15: Horizontal stress, σ_x, change around the created crack (Liu 2015).

A typical MTFHW completion includes multiple hydraulic fracture stages, each with multiple perforation clusters, each of which is intended to initiate and propagate a hydraulic fracture. The industry tends to use more perforation clusters per stage to enhance the tendency to create shear fractures near the main tensile crack. Thus, the distance between each hydraulic fracture is short, usually below 100 ft, and as short as 15-20 ft. When the fractures are within 100 ft away in horizontal direction, the stress alteration will be as much or more than that shown in Figure 15 and could even exceed the maximum principle stress. Thus, we can consider this stress elevation as a stress barrier.

The stress elevation occurs in formation rock that may contain natural fractures. The presence of natural fractures is especially likely in a source rock formation because primary and/or secondary hydrocarbon migration likely occurred through natural fractures. Current sourcing activity would impact conductivity of existing natural fractures, but experience has shown they are not sufficiently conductive to support production without hydraulic fracture stimulation. Microseismic surveys detect acoustic activity generated mainly by shear motion likely occurring in existing natural fractures that occurs as a result of stress elevation from hydraulic fracture creation. Increase in the bulk permeability of a natural fracture network may occur via shear dilation (Barton et al., 1985).

A further question relates to stress relaxation. The time frame for relaxation of the stress elevation near a MTFHW is likely to be very long, despite what might be presumed from models like that shown in Figure 16 from Manchanda (Manchanda et al., 2014). Such figures have been shown to justify impairment in successive hydraulic fractures along a horizontal well due to so-called stress shadowing and have motivated interest in estimating instantaneous shut-in pressure (ISIP) from treatment falloff data (Hurd and Zoback 2012). However, the drop in stress elevation shown in Figure 16 relates to one fracture, not multiple parallel fracture planes generated essentially simultaneously in one fracture stage. It is especially important to note that Figure 15 and Figure 16 show stress elevation extent in the direction normal to the fracture that is much greater than the typical distance between created hydraulic fractures. In any case, studies like that by Hurd and Zoback 2012 show evidence of stress alteration over longer time frames than that shown in Figure 16.

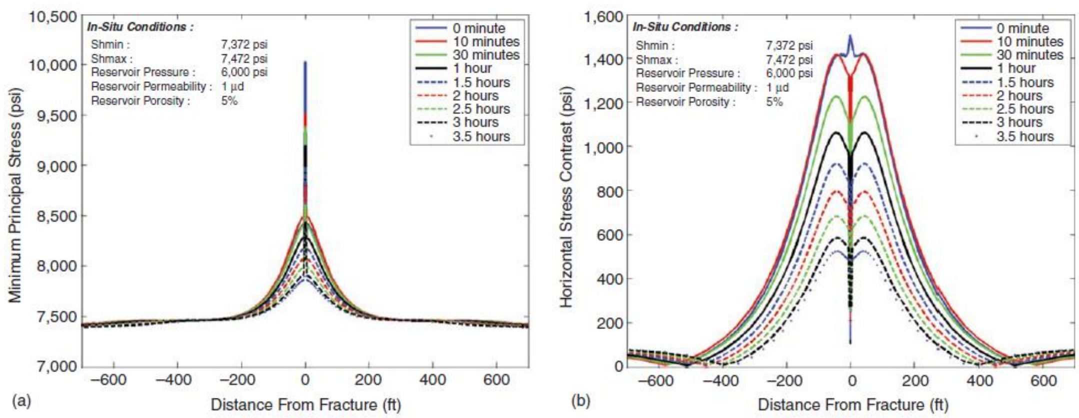

Figure 16: a) Changes in the local-reservoir minimum principle stress because of fracture closure and pressure mitigation from the closing fracture. b) changes in the local reservoir horizontal-stress contrast because of fracture closure and pressure migration from the closing fracture. The fracture is located at 0 ft in the figure (Manchanda et al., 2014).

Until well flowback production, the only way stress can relax is via leakoff of the treatment fluid into very low matrix or effective bulk secondary permeability, and presence of proppant further slows stress dissipation. Hence, we hypothesize that sufficient stress elevation remains near a recently hydraulically fractured well to justify the model discussed in the next section.

3.1.2. Asymmetric Fracturing Model Derivation

The purpose of our model is to simulate uneven hydraulic fracture growth due to lateral change in minimum stress in the direction of the fracture propagation. Figure 17 shows a gun barrel view of two horizontal wells, HW 1 and HW 2; a) shows a uniform stress, σ_0, before any fracture treatment; b) shows symmetric fracture planes propagated during the treatment in HW1 elevating the original balanced stress to σ_1 on each side of the well; c) shows the hydraulic fracture of HW2 becomes longer on the right side because stress on the right side is smaller, $\sigma_0 < \sigma_1$, and, therefore, easier to break.

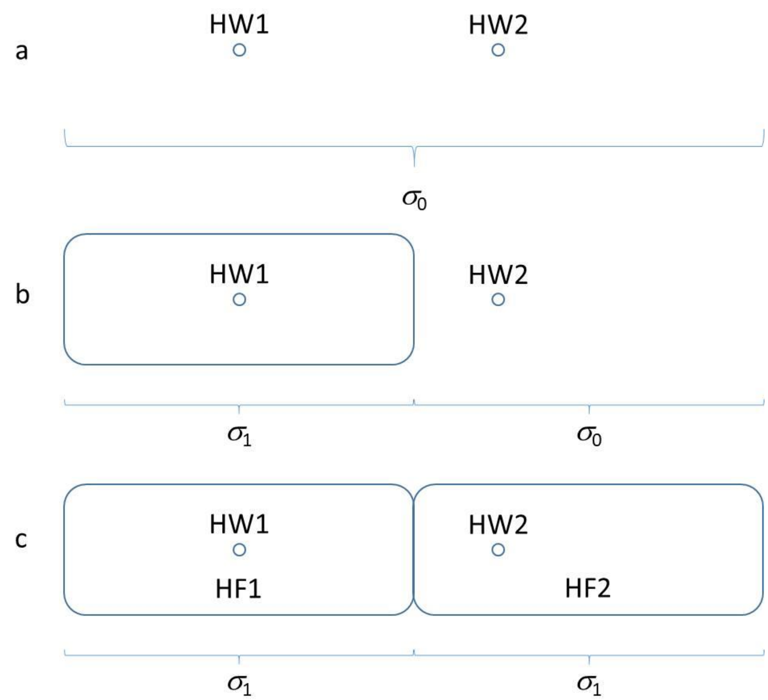

Figure 17: a) Initial 2 horizontal wells with uniform lateral minimum stress; b) symmetric fractures in first horizontal well elevate minimum stress; c) asymmetric fractures in second horizontal well.

For constant rate fracturing treatment under a uniform stress condition, Nolte (1979, 1986) proposed the following model for fracture propagation with time. He started with the power law relationship between fracture area and the elapsed time

$$\frac{A_{f0}}{A_{f1}} = \left(\frac{t_0}{t_1}\right)^{\alpha}, \tag{4}$$

where Δt_0 and Δt_1 are the two elapse times at any given time, A_{f0} and A_{f1} are the correspondent fracture area, and α is area exponent constant before and after shut-in.

According to material balance function, the total pumping volume of any given time, t_i, with constant pumping rate, q_i, can be expressed as

$$V_{total} = q_i t_i = V_f + V_{leakoff}, \tag{5}$$

where V_{total} is the total pumping volume; V_f is the created fracture volume; $V_{leakoff}$ is the leak-off volume. Further, Nolte (1979, 1986) specified that

$$V_f = A_f c_f \Delta p_{net} \quad \text{and} \tag{6}$$

$$V_{leakoff} = 2 r_p c_L \sqrt{t_i} A_f g_0, \tag{7}$$

where Δp_{net} is the net pressure; c_f is fracture compliance; r_p is ratio of permeable fracture surface area to the gross fracture area; c_L is the leak-off coefficient; $g(\alpha, \Delta t_D)$ is the loss-volume function and g_0 is when $g(\alpha, \Delta t_D)$ at $\Delta t_D = 0$. Liu and Ehlig-Economides (Liu and Ehlig-Economides 2019) provided values or expressions of c_f, α and g_0 reproduced in Table 1.

Table 1: Fracture compliance, $g_{0,}$ β and α_s for different fracture models

Fracture model	PKN	KGD	Radial
Fracture compliance (c_f)	$\frac{\pi\beta_s h_f}{2E'}$	$\frac{\pi\beta_s x_f}{E'}$	$\frac{16\beta_s R_f}{3\pi E'}$
g_0	1.41	1.48	1.38
β_s	$4/5$	0.9	$33\pi^2/32$
α	4/5	2/3	8/9

Finally, Nolte (Nolte 1979, 1986) rewrote Equation (3):

$$q_i t_i = A_{ft} c_f \Delta p_{net} + 2r_p c_L \sqrt{t_i} A_{ft} g_0 \,, \tag{8}$$

equation (6) enables calculation of the fracture net pressure as a function of time for constant rate injection. Assuming that the fractures are created under uniform stress with the same fracture height, h_f, we have

$$A_{ft} = A_{fl} + A_{fr} = h_f(x_{fl} + x_{fr}) \,, \tag{9}$$

where A_{fl} is the left fracture area and A_{fl} is the right fracture area; x_{fl} is the left fracture length, and x_{fr} is the right fracture length. Because continued pumping can propagate the fracture to the right at fracture pressure less than the elevated stress to the left, fracture growth to the left will stop, leaving

$$x_{fl} \le D, \tag{10}$$

where *D* is the distance between HW2 and the elevated stress zone around HW1.

With total fracture area A_f calculated from Equation (8), we can calculate the fracture net pressure and fracture lengths from each side of the well at any given time from Equation (7):

$$\begin{cases} x_{fr} = x_{fl} = \frac{A_{ft}}{2h_f}, \text{for } x_{fl} < D \\ x_{fr} = \frac{A_{ft}}{h_f} - D, \text{for } x_{fl} = D \end{cases}. \tag{11}$$

The next section shows results generated by our fracture model.

3.2. Modeling Results

As shown in Figure 17, we assume there are two horizontal wells in the formation, the wellbore spacing is 900 ft, and the length of recent fractures from HW1, x_f, is 600 ft. Therefore, we can easily calculate that the distance from HW2 to the stress barrier, d, is 300 ft. Additional parameters are shown in Table 2:

Table 2: Input parameters for synthetic model

Parameter	Value
q, bbl/min	25
h_f, ft	100
t_p, min	120
E', psi	6×10^6
c_L	5×10^{-4}
x_f, ft	600
d, ft	300
Model	KGD

The simulated results are shown in Figure 18. The hydraulic fractures grow symmetrically before reach the stress boundary, then the fractures grow towards the right side of the well where the stress is lower.

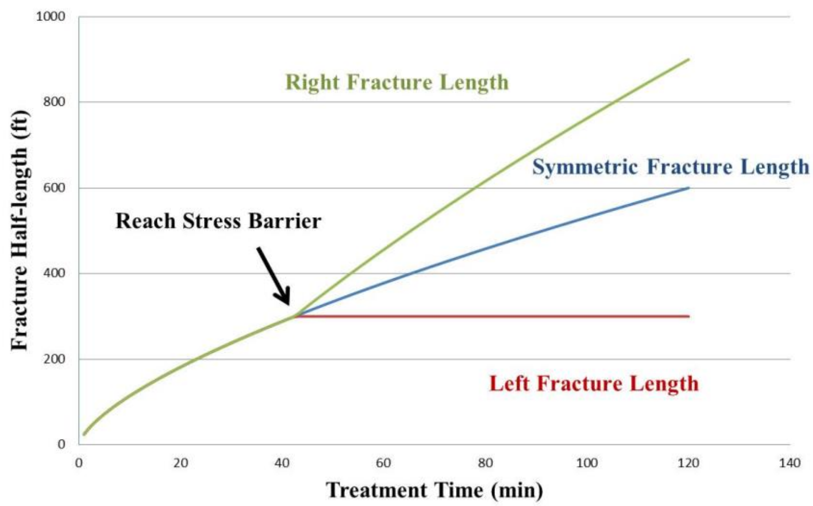

Figure 18: Simulated asymmetric fracture growth against time. The blue line represents fracture half-length under asymmetric lateral stress condition; red and green lines represent asymmetric fracture growth from left and right, respectively.

As mentioned in section 1.1.2, the presence of asymmetric fractures can have negative impact on well performance. There are a couple of factors that could affect the well productivity. Proppant transport is one of key factors determining the effective propped lengths and therefore the productivity of these fractured wells (Gadde and Sharma 2005). We will use a simple proppant model to simulate the propped fracture length under stress imbalance.

We rewrite Equation (8) to calculate propped slurry volume related to propped fracture volume and leak-off volume as

$$q_i t_{i,prop} = A_{ft,prop} c_f \Delta p_{net} + 2 r_p c_L \sqrt{t_i} A_{ft,prop} g_0 , \tag{12}$$

where $t_{i,prop}$ is the propped slurry pumping time; $A_{ft,prop}$ represents the propped fracture area. We assume constant slurry rate and constant proppant concentration. We also assume the fracture compliance, c_f, and leak-off coefficient, c_L, are not affected by adding proppant, and that therefore they remain the same. The net pressure, Δp_{net}, can be computed at any given time from Equation (8) by using fracture length calculated from Equation (11). Therefore, the propped fracture area, $A_{ft,prop}$, can be calculated from which the proppant fracture length can be obtained.

In this case, we consider two scenarios, proppant injection starts before the left fracture reaches the stress barrier and proppant injection starts after the left fracture reaches the stress barrier. The simulated results are shown in Figure 19 and Figure 20.

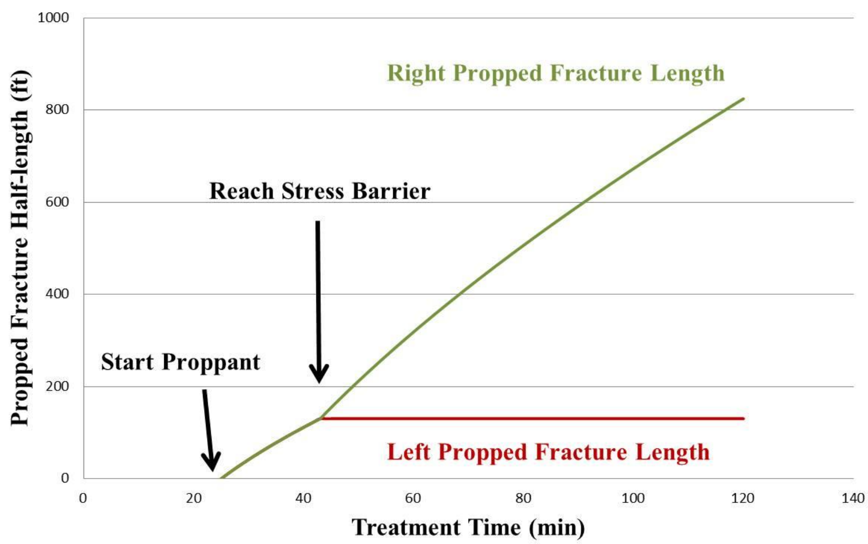

Figure 19: Proppant injection starts after 25 minutes of pad injection, left fracture reaches stress barrier around 43 minutes after fracturing started.

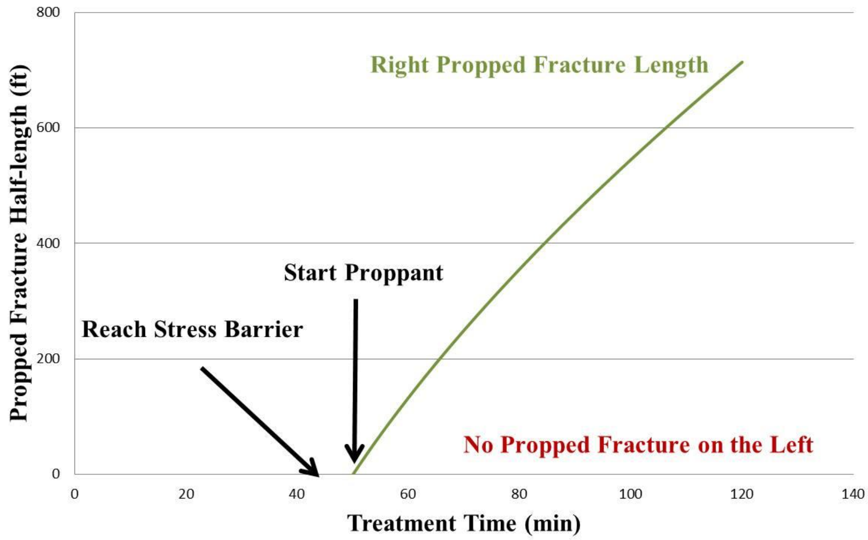

Figure 20: Proppant injection starts after 50 minutes of pad injection, left fracture reaches stress barrier around 43 mins after fracturing started.

The results suggests that in the first case proppant transport is arrested in the left fracture wing when the left fracture reaches the stress barrier, and the remaining proppant will be transported towards the right side which has lower stress. In the second case, all the proppant will be transported towards the right fracture.

3.3. Summary

In this chapter, we have presented an adapted 2-D fracture model to simulate asymmetric fracture propagation by redistributing the volume of injected fluid on each side of the wellbore to allow uneven hydraulic fracture growth. The model is computationally fast and easy to use. We also simulated propped fracture length by using a simple constant rate, constant proppant concentration model. The results suggest that propped fracture length will also be asymmetric.

In next chapter, we will discuss implications of our fracture model for optimization of hydraulic fracturing treatments in multiple wells.

CHAPTER 4

Hydraulic Fracturing Treatment Optimization

Chapter 1 showed evidence from microseismic case studies that hydraulic fractures in a second well grew away from a nearby previously fractured well, resulting in unequal fracture wing lengths. Also, the fracture azimuth from successive stages stayed the same instead of bending as predicted by some models for successive fracture stages. We also noted in Chapter 1 that asymmetric fractures adversely impact well performance. This also served as a key rationale for conducting this research. Chapter 2 explained why so little evidence of asymmetric fracture growth has been published.

Chapter 3 derived a 2-D hydraulic fracture model that simulates asymmetric fracture propagation when the formation stress is not uniform laterally. We have noted previously that asymmetric fractures can reduce the performance of affected wells. Thus, the asymmetric fractures should be avoided if possible. The next two sections provide recommendations to avoid or mitigate effects of asymmetric fractures.

4.1. Change Well Completion Sequence

The model in Chapter 3 shows that fracturing one well after another risks asymmetric fracture propagation. A way to avoid this problem is to space the wells farther apart. Figure 21 illustrates the result for two wells spaced sufficiently far apart that the stress elevated stress zones for the wells do not intersect, and both wells have symmetric fractures.

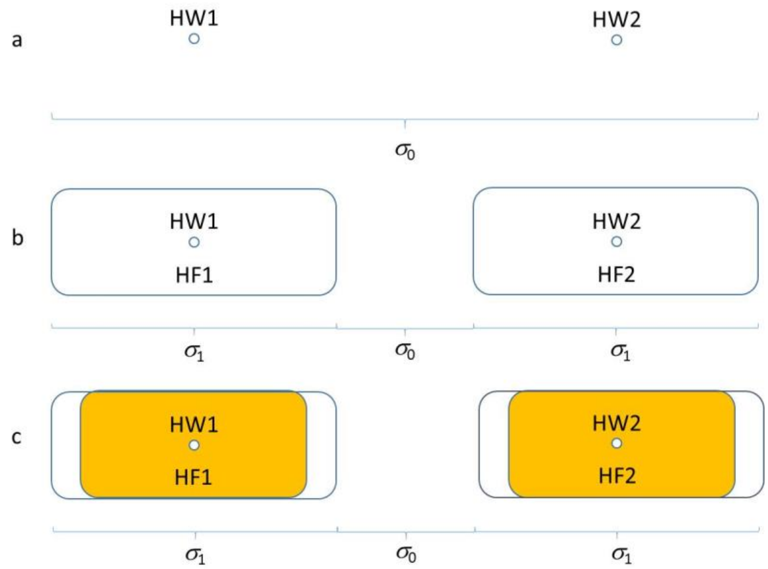

Figure 21: Show a case that two wells are far apart. a) Initial 2 horizontal wells with uniform lateral minimum stress; b) symmetric fractures in both horizontal wells; c) symmetric propped fractures in both wells.

The final diagram in this figure, labeled c, indicates how far proppant may penetrate in the created fractures. The propped region will also be symmetric, but there may be a significant gap between propped fracture regions.

Figure 22 illustrates the likely propped regions for the case shown in Figure 17. In this case proppant flow toward the previously fractured well could be severely limited because flow of the pad fluid may stop before pumping of the proppant slurry starts. In such a case the proppant slurry would flow in the other direction. However, the extended reach of the proppant is not guaranteed. This suggests even further detriment could be caused by the asymmetric fracture propagation.

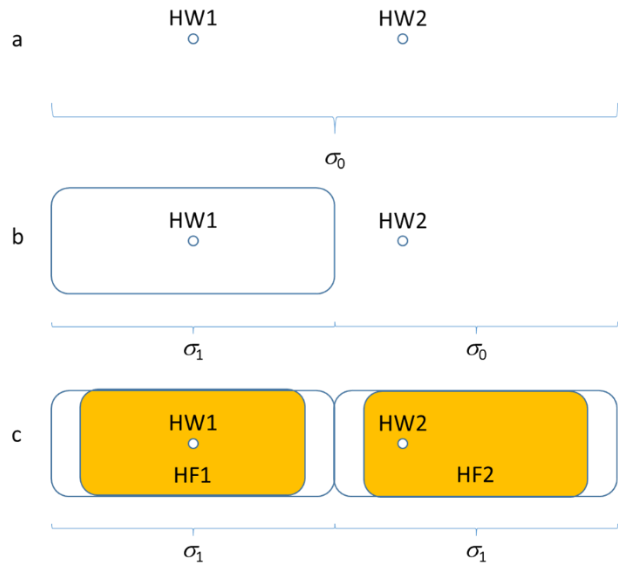

Figure 22: Show a case that two wells are close. a) Initial 2 horizontal wells with uniform lateral minimum stress; b) symmetric fractures in first horizontal well elevate minimum stress; c) asymmetric propped fractures in second horizontal well.

The gap between propped regions in Figure 21 can be remedied by drilling a well HW3 between HW1 and HW2, as shown in Figure 23. In this case the first part of the hydraulic fracture treatment will be similar to the other two wells, as shown in c. When the fracture wings propagate into the elevated stress zones, the pumping pressure must be increased to maintain the fracture net pressure. However, because the stress alteration is symmetric, both fracture wings can continue to propagate, as in c'. The final diagram at the bottom of this figure suggests symmetric proppant distribution may also be possible.

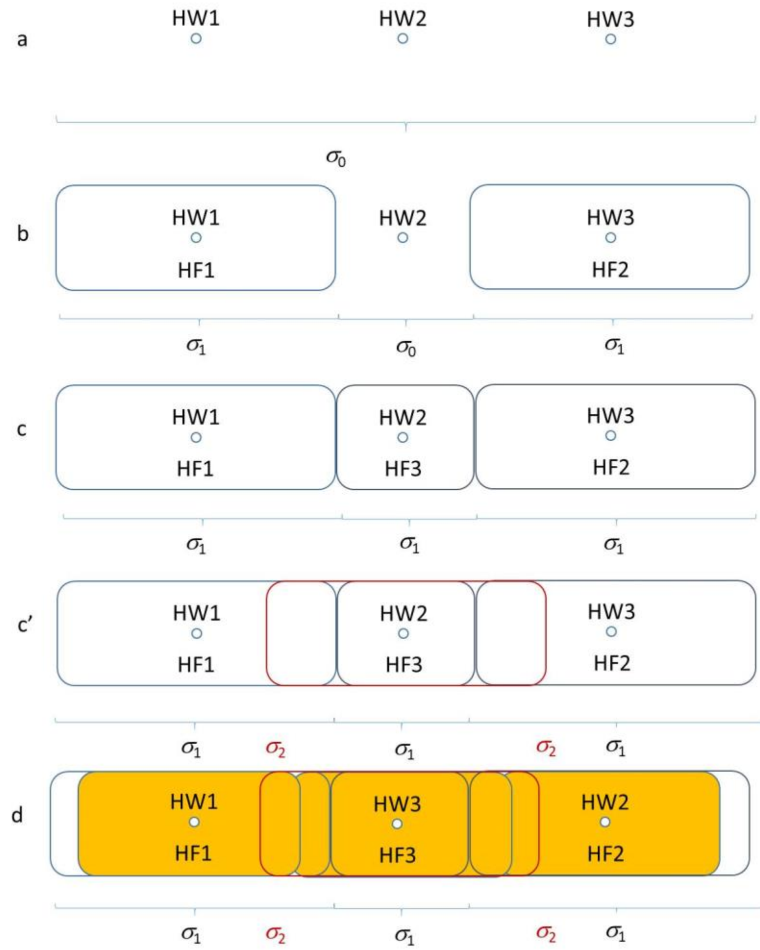

Figure 23: Show a case that has three wells. a) Initial 3 horizontal wells with uniform lateral minimum stress; b) symmetric fractures in first and third horizontal well elevate minimum stress; c) symmetric fractures in second horizontal well before reach the stress barrier; c') by increasing treatment pressure, fracture can still grow symmetrically; d) symmetric propped fractures in all three wells.

Before leaving this section, it is worth mention that it recommends an approach that is quite inconsistent with recommendations proposed by Thompson (Thompson et al., 2018) that are shown in Figure 22. Our results suggest the pressure wall will cause asymmetric fracture growth in the completing (hydraulic fracturing) of the next well. Unless the created fractures have very high conductivity, this approach would cause all succeeding wells to have suboptimal well performance.

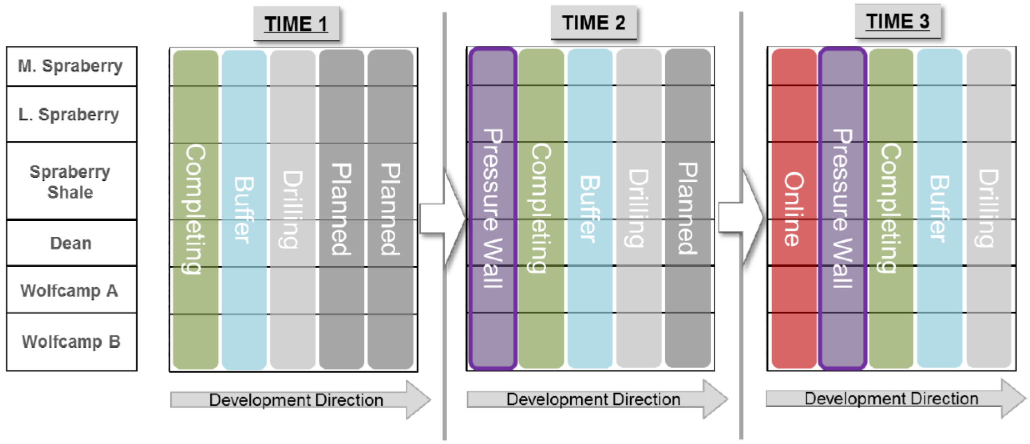

Figure 24: Tank model development approach proposed by Thompson (Thompson et al., 2018).

We suggest for multi-well fracturing treatment, instead of fracturing one boundary well first, the operators could consider fracture two boundary wells together as shown in Figure 25. This case is very similar to the case described in Figure 23, except having more wells. To fracture two boundary wells first and then fracture every other well in the middle could allow the operators to balance the stress. Therefore, asymmetric fractures can be avoided. More importantly, the propped fractures are symmetric.

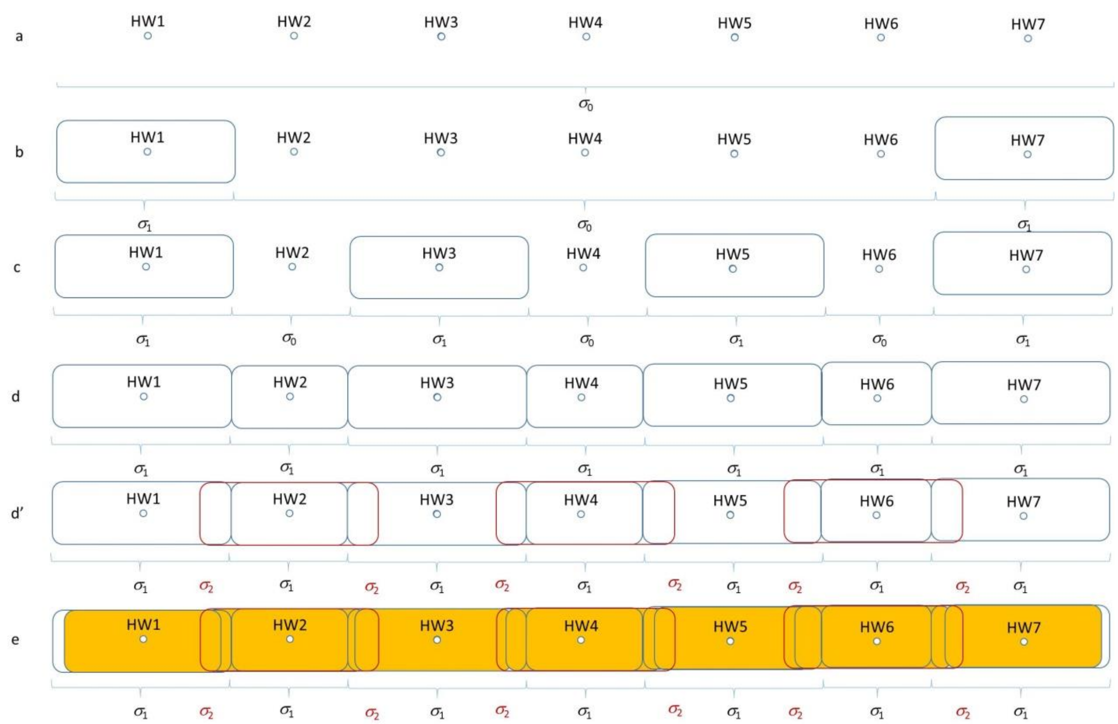

Figure 25: Multi-well treatment design. a) Initial 7 horizontal wells with uniform lateral minimum stress; b) symmetric fractures in first and seventh horizontal well elevate minimum stress; c) symmetric fractures in third and fifth horizontal wells; d) symmetric fractures in the second, fourth and sixth wells before reach the stress barrier; d') by increasing treatment pressure, fracture can still grow symmetrically; e) symmetric propped fractures in all seven wells.

4.2. Increase Fracture Conductivity

If asymmetric fracture growth cannot be avoided, results from Walser and Siddiqui 2016 suggest that ensuring sufficient fracture conductivity will mitigate much of the well performance impairment resulting from the asymmetric fractures.

4.3. Implicate of Frac Hits

A frac hit is often described as well interference that will cause production losses in parent-child wells. The evidence of a frac hit can be found by recovering parent well water tracer in the child well (King et al., 2017). It could be also confirmed by microseismic surveys that fractures grow asymmetrically toward to the parent well, as shown in Figure 2. To avoid frac hits, operators try to pressure up the parent well or the wells between the parent well and the wells that are being treated (Thompson et al., 2018; Whitfield et al., 2018), but generally operators have found that frac hits cannot be stopped just by shutting in or simply pressuring up existing wells (King et al., 2017). In addition to that, our modeled results from Chapter 3 indicated that pressuring up existing wells could create a stress barrier that would cause asymmetric fractures to be formed in the opposing direction, still resulting in suboptimal well performance. Based on our modeled results (Figure 22 and Figure 23), we suggest that the operators need to stop the asymmetric fractures in the first place by changing the fracturing sequence.

For wells treated at the same time, a frac hit is not necessarily a problem, and it could be an indicator that fractures touch. Therefore, it provides a direct signal of what the maximum well spacing should be (Cao et al., 2017). Figure 26 shows that there is no gap between fractures due to frac hit. Our modeled results suggested that the operators should still keep pumping until propped fractures touch because unpropped fractures will close after initial production and result in a gap in the stimulation.

Figure 26: Illustration of completion fluid interaction due to frac hit (Cao et al., 2017).

Therefore, we could use frac hit as a diagnostic tool to confirm that the fractures touch. If all the wells are treated together, the operators need to keep pumping until frac hits are observed. If the nearest well is on production or depleted, the operators should stop pumping when a frac hit occurs. To confirm fracture to fracture connection, bottom hole pressure from monitor well could be used as an indicator of frac hit, as shown in Figure 27 (Daneshy 2017). Snit (Sani et al., 2015) further recommended using pressure responses along with proppant tracers and fluid tracers as a diagnostic tool to provide a significant understanding of fracture geometry including proppant coverage.

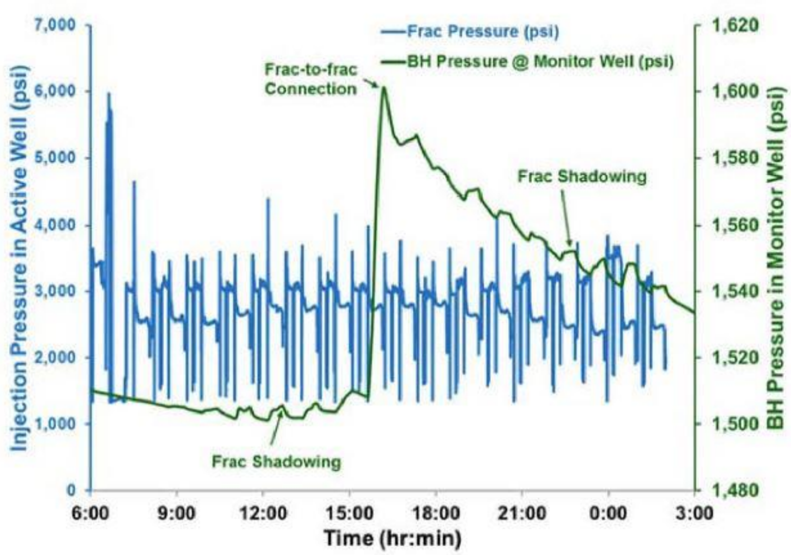

Figure 27: Frac hit could be found from pressure data from monitor well (Daneshy 2017).

4.4. Summary

In this chapter, we have discussed the impact of asymmetric fractures, how to improve the hydraulic fracture design to avoid asymmetric fractures and to design for high fracture conductivity when asymmetric fracturing is unavoidable. We also suggested to avoid detrimental frac hits in parent-child wells by changing the fracturing sequence. For the wells treated at the same time, we could use frac hit as a diagnostic tool to avoid gaps between fractures.

CHAPTER 5

Results, Conclusions and Discussion

This chapter will summarize the thesis results and conclusions apparent from the previous chapters. We will also discuss several key aspects of our assumptions, observations and applications.

5.1. Results and Conclusions

In this thesis, we have concluded:

1) Microseismic surveys show evidence that hydraulic fractures grow away from a recently fractured well.
2) Stress elevation from hydraulic fracturing will not relax until well flowback.
3) Asymmetric fracture growth in a well near a recently fractured well occurs because of the elevated formation stress caused by fracturing the first well.
4) In addition to productivity loss and reduced EUR, MTFHWs with asymmetric fractures may also leave unpropped space between wells.
5) Asymmetric fracture growth can be avoided by ordering well fracturing operations to space wells far enough apart to avoid fracturing into elevated stress and then fracture an infill well to avoid any gap between propped SRVs.
6) When asymmetric hydraulic fractures are expected, the fracture design should target high fracture conductivity to mitigate reduced well performance resulting from asymmetric fractures.

7) In a parent-child well relation, frac hit could be stopped by changing fracturing sequence. When the wells are treated in the same time, frac hit could be used a diagnostic tool to avoid gaps between fractures.

5.2. Future Work

In this thesis, we have made assumptions that merit further comment. The following sections highlight four key points: single fracture assumption in the 2-D fracture model, modeling formation stress relaxation, production affected by asymmetric fractures, and fracturing nearly depleted wells.

5.2.1. Model for Simultaneous Propagation of Multiple Fractures

The horizontal stress elevation caused by opening of a fracture might underestimate the actual elevated stress under typically operations because usually multiple perforation clusters are shot in each fracture stage. The stress alteration distribution showed in Figure 15 is computed based on a single fracture opening.

When multiple fractures are pumped simultaneously, the stress elevation is expected to be much higher. Modeling the stress elevation magnitude caused by multiple fractures could help estimate the location of the created stress barrier. This information could be used to adjust well spacing, and treatment size accordingly.

Real-time microseismic monitoring can be used to calibrate such a model. The fracturing treatment plans could be adjusted from estimated fracture length and width observed from microseismic results. Then, potential asymmetric fracturing could be reduced or avoided.

5.2.2. Model Formation for Stress Relaxation

A future study could rigorously model the stress relaxation for multiple fractures generated simultaneously from multiple perforation clusters in the same fracture stage. In particular, in addition to stress relaxation, there should be additional attention to stress reorientation. A more rigorous stress relaxation model could provide insight on the effect of elevated stress on successive fracture stages that may be more consistent with microseismic evidence than the curved fractures like those shown by Nagel (Nagel et al., 2013), which relate both to stress reorientation than to stress elevation.

5.2.3. Asymmetric Fractures and Production

Walser and Siddiqui (2016) have modeled cumulative production by shifting fracture 200 ft towards one side. But the fracture width and conductivity of uneven fractures can be different and will influence the productivity of the affected wells. Therefore, we could develop a more rigorous model for forecasting production from asymmetric fractures caused by non-uniform stress distribution.

5.2.4. Fracturing Near Depleted Wells

This thesis has focused on asymmetric fractures caused by elevated formation stress. However, our method and theory also could be implemented for hydraulic fracturing near a depleted well. As mentioned by Walser and Siddiqui (2016), the depleted well could lower the formation stress near it and would also cause stress imbalance. We could use our model to optimize the well sequencing to minimize the number of wells adversely impacted by stress imbalance.

References

Barton, N., Makurat, A., Vik, G., & Loset, F. (1985). The modelling and measurement of super-conducting rock joints. *26th US Symposium on Rock Mechanic*, (June), 487–496.

Cao, R., Li, R., Girardi, A., Chowdhury, N., & Chen, C. (2017). Well Interference and Optimum Well Spacing for Wolfcamp Development at Permian Basin. *Unconventional Resources Technology Conference*. http://doi:10.15530/URTEC-2017-2691962

Cipolla, C. L., Mack, M. G., Maxwell, S. C., & Downie, R. C. (2011). A Practical Guide to Interpreting Microseismic Measurements. *North American Unconventional Gas Conference and Exhibition*, (June), 14–16. http://doi.org/10.2118/144067-MS

Daneshy, A. (2017). Aggressive Fracturing Treatments in Horizontal Wells: Benefits and Pitfalls. *Society of Petroleum Engineers*. http://doi:10.2118/187147-MS

Duncan, P. M., (2010). Microseismic Monitoring - Technology State of Play. *Society of Petroleum Engineers*. http://doi:10.2118/131777-MS

Duncan, P. M., & Eisner, L. (2010). Reservoir Characterization Using Surface Microseismic Monitoring. *Geophysics*, 75(5), 75A139-75A146. https://doi-org.ezproxy.lib.uh.edu/10.1190/1.3467760

Economides, M. J., & Nolte, K. G. (2000). *Reservoir stimulation*. Chichester, England: Wiley.

Gadde, P. B., & Sharma, M. M. (2005). The Impact of Proppant Retardation on Propped Fracture Lengths. *SPE Annual Technical Conference and Exhibition*. http://doi.org/10.2118/97106-MS

Gaurav, A., & Kashikar, S. (2015). Stimulated rock volume and estimated ultimate recovery. *Society of Petroleum Engineers - Unconventional Resources Technology Conference, URTeC 2015*, (July), 20–22. http://doi.org/10.15530/urtec-2015-2131921

Gupta, J., Zielonka, M., Albert, R. A., El-Rabaa, A. M., Burnham, H. A., & Choi, N. H. (2012). Integrated Methodology for Optimizing Development of Unconventional Gas Resources. *Society of Petroleum Engineers*. http://doi:10.2118/152224-MS

Hurd, O., & Zoback, M. D. (2012). Stimulated Shale Volume Characterization: Multiwell Case Study from the Horn River Shale: I. Geomechanics and Microseismicity. *SPE Annual Technical Conference and Exhibition*, *C*. http://doi.org/10.2118/159536-MS

King, G. E., Rainbolt, M. F., & Swanson, C. (2017). Frac Hit Induced Production Losses: Evaluating Root Causes, Damage Location, Possible Prevention Methods and Success of Remedial Treatments. *Society of Petroleum Engineers*. http://doi:10.2118/187192-MS

Liu, G. (2015). *Before-closure analysis of fracture calibration test.* Available from ProQuest Dissertations & Theses Global; SciTech Premium Collection. Retrieved from http://search.proquest.com.ezproxy.lib.uh.edu/docview/1739170811

Liu, G., & Ehlig-Economides, C. (2019). Comprehensive Before-closure Model and Analysis for Fracture Calibration Injection Falloff Test, *Journal of Petroleum Science and Engineering*. https://doi.org/10.1016/j.petrol.2018.08.082

Manchanda, R., Sharma, M. M., & Holzhauser, S. (2014). Time-Dependent Fracture-Interference Effects in Pad Wells. *SPE Production & Operations*, *29*(04), 274–287. http://doi.org/10.2118/164534-PA

Maxwell, S. (2012). Comparative Microseismic Interpretation of Hydraulic Fractures. *SPE Canadian Unconventional Resources Conference*, (November), SPE 162782. http://doi:10.2118/162782-MS

McKenna, J. (2014). Verification of a Proppant-Filled Discrete Fracture Network Model, *SPE Western North American and Rocky Mountain Joint*, PE-169496-MS. https://doi-org.ezproxy.lib.uh.edu/10.2118/169496-MS.

Nagel, N. B., Zhang, F., Sanchez-Nagel, M. A., & Lee, B. (2013). Evaluation of Stress Changes Due to Multi-Stage Hydraulic Fracturing – Consideration of Field Results. *ISRM International Symposium - EUROCK 2013*, 941–946.

Newberry, B. M., Nelson, R. F., & Ahmed, U. (1985). Prediction of Vertical Hydraulic Fracture Migration Using Compressional and Shear Wave Slowness. *SPE/DOE Low Permeability Gas Reservoirs Symposium*, 8. http://doi.org/10.2118/13895-MS

Nolte, K. (1979). Determination of Fracture Parameters from Fracturing Pressure Decline, *SPE Annual Technical Conference and Exhibition*. SPE-8341-MS. https://doi-org.ezproxy.lib.uh.edu/10.2118/8341-MS

Rahman, M. M., & Rahman, M. K. (2010). A Review of Hydraulic Fracture Models and Development of An Improved Pseudo-3D Model for Stimulating Tight Oil/Gas Sand. *Energy Sources, Part A: Recovery, Utilization and Environmental Effects*, *32*(15), 1416–1436. http://doi.org/10.1080/15567030903060523

Sani, A. M., Podhoretz, S. B., & Chambers, B. D. (2015). The Use of Completion Diagnostics in Haynesville Shale Horizontal Wells to Monitor Fracture Propagation, Well Communication, and Production Impact. *Society of Petroleum Engineers*. doi:10.2118/175917-MS

Sneddon, I. N., & Elliot, H. A. (1946). The Opening of a Griffith Crack Under Internal Pressure. *Quart. Appl. Math*, *4*(3), 262–267. http://doi.org/10.1016/S1043-2760(98)00144-1

Sneddon, I. & Elluitt, H., (1946). The Opening of a Griffith Crack under Internal Pressure, *Quarterly of Applied Mathematics*, 4 (3): 262-267.

Stephenson, B., Galan, E., Williams, W., MacDonald, J., Azad, A., Carduner, R., & Zimmer, U. (2018). Geometry and Failure Mechanisms from Microseismic in the Duvernay Shale to Explain Changes in Well Performance with Drilling Azimuth. *Society of Petroleum Engineers*. http://doi:10.2118/189863-MS

Tan, Y. (2015). *Study of microseismic events: Their source mechanism, spatial and temporal distribution, and the evolution of transmitting medium.* Available from ProQuest Dissertations & Theses Global. (2018825679). Retrieved from http://search.proquest.com.ezproxy.lib.uh.edu/docview/2018825679

Thompson, J., Franciose, N., Schutt, M., Hartig, K., & McKenna, J. (2018). Tank Development in the Midland Basin, Texas: A Case Study of Super-Charging a Reservoir to Optimize Production and Increase Horizontal Well Densities, *Unconventional Resources Technology Conference*,. URTEC-2902895-MS. https://doi-org.ezproxy.lib.uh.edu/10.15530/URTEC-2018-2902895

Walser, D., & Siddiqui, S. (2016). Quantifying and Mitigating the Impact of Asymmetric Induced Hydraulic Fracturing from Horizontal Development Wellbores. *SPE Annual Technical Conference and Exhibition*. http://doi.org/10.2118/181656-MS

Warpinski, N. R., Wolhart, S. L., & Wright, C. A. (2001). Analysis and Prediction of Microseismicity Induced by Hydraulic Fracturing. *SPE Annual Technical Conference and Exhibition*. http://doi.org/10.2118/71649-MS

Warpinski, N. R., Mayerhofer, M. J., & Agarwal, K. (2013). Hydraulic Fracture Geomechanics and Microseismic Source Mechanisms. *SPE Journal*, *18*(4), 766–780. http://doi.org/10.2118/158935-PA

Whitfield, T., Watkins, M. H., & Dickinson, L. J. (2018, September 17). Pre-Loads: Successful Mitigation of Damaging Frac Hits in the Eagle Ford. *Society of Petroleum Engineers*. http://doi:10.2118/191712-MS.